Heterogeneous Hydrogenation Hot Paper

International Edition: DOI: 10.1002/anie.201602512
German Edition: DOI: 10.1002/ange.201602512

Pt_3Co Octapods as Superior Catalysts of CO_2 Hydrogenation

Munir Ullah Khan[+], Liangbing Wang[+], Zhao Liu[+], Zehua Gao, Shenpeng Wang, Hongliang Li, Wenbo Zhang, Menglin Wang, Zhengfei Wang, Chao Ma, and Jie Zeng**

Abstract: *As the electron transfer to CO_2 is a critical step in the activation of CO_2, it is of significant importance to engineer the electronic properties of CO_2 hydrogenation catalysts to enhance their activity. Herein, we prepared Pt_3Co nanocrystals with improved catalytic performance towards CO_2 hydrogenation to methanol. Pt_3Co octapods, Pt_3Co nanocubes, Pt octapods, and Pt nanocubes were tested, and the Pt_3Co octapods achieved the best catalytic activity. Both the presence of multiple sharp tips and charge transfer between Pt and Co enabled the accumulation of negative charges on the Pt atoms in the vertices of the Pt_3Co octapods. Moreover, infrared reflection absorption spectroscopy confirmed that the high negative charge density at the Pt atoms in the vertices of the Pt_3Co octapods promotes the activation of CO_2 and accordingly enhances the catalytic activity.*

The reduction and fixation of CO_2 into useful chemicals and fuels has attracted tremendous interest to meet current energetic and environmental demands.[1–3] Considering the high stability of a CO_2 molecule with a bond length of 116.3 pm and a bond dissociation energy of 1072 kJ mol^{-1}, the activation of CO_2 plays a pivotal role in the chemical transformation of CO_2. Thanks to a variety of efforts, the electron transfer to CO_2, with an associated energy of about 0.6 eV, is generally considered as the crucial step during the activation of CO_2 from both theoretical and experimental perspectives.[4–8] This process can be realized through heterogeneous catalysis where the catalytic performance is largely determined by the electronic properties of the surface. Typical heterogeneous catalysts for the transformation of CO_2 include Pt, Au, Ru, Cu, and their alloys. For example, Tsang and co-workers discovered that the interaction of Cu and ZnO/CdSe at heterojunctions increases the negative charge density of Cu, facilitating the activation of CO_2.[5] Chen et al. reported that the electronic polarization at the interface between Au and a CeO_x/TiO_2 substrate could generate active centers for CO_2 adsorption.[6] Another notable example is the interface between Cu and CeO_2, which was found to be significantly active in the transformation of CO_2 into $CO_2^{\delta-}$, revealing remarkable catalytic performance in CO_2 hydrogenation.[7] Recently, a model system was reported by Calaza and co-workers to shuttle electrons back and forth between Au and adsorbed CO_2 through a MgO film to induce the formation of a CO_2 anion radial.[8] Therefore, it is of significant importance to develop approaches to engineer the electronic properties of heterogeneous catalysts to improve their performance in CO_2 hydrogenation.

One strategy to modulate the electronic properties of catalysts is to control their shapes because of the dependence of the charge distribution on the morphology. For example, according to Bader charge calculations of metal nanopolyhedra, electrons are preferentially accumulated at tips and edges.[9] Accordingly, highly branched nanocrystals such as multipods and nanodendrites with multiple tips are expected to benefit from the accumulation of electrons in their tips. Another strategy for electronic modification is to form an alloy by adding another metal; charge transfer will then occur owing to the different electronegativities of the constituent metals.[10] As such, electrons tend to be donated from metal atoms with lower electronegativity to more electronegative metals.

Herein, we combined these two strategies to modulate the electronic properties of Pt_3Co nanocrystals for enhanced catalytic performance in the CO_2 hydrogenation to methanol. During CO_2 hydrogenation, Pt_3Co octapods exhibited the highest turnover frequency (TOF) of 758 h^{-1}, which was 2.2, 6.1, and 6.6 times higher than that of Pt_3Co nanocubes, Pt octapods, and Pt nanocubes, respectively. The remarkable activity of Pt_3Co octapods is due to sharp-tip and alloy effects, both of which contributed to the accumulation of negative charges on the Pt atoms at the vertices. Moreover, the activation of CO_2 to form a $CO_2^{\delta-}$ intermediate was directly observed by infrared reflection absorption spectroscopy (IRRAS). The ability to activate CO_2 was correlated with the negative charge densities of the Pt atoms in these catalysts.

In a typical synthesis of Pt_3Co octapods, $Co(acac)_2$, $Pt(acac)_2$, and octanethiol were dissolved in a solution containing octadecene and oleylamine. The mixture was heated in an oil bath at 170 °C for 30 min. Figure 1 A and 1 B show representative transmission electron microscopy (TEM) and high-angle annular dark-field scanning TEM (HAADF-STEM) images of the as-obtained octapods, indicating the formation of uniform eight-armed star-like nanocrystals with an average size of 13 nm in high purity (Supporting Information, Figure S1). The detailed morphological characteristics of the octapods were fully examined by HAADF-STEM and their corresponding fast Fourier transform (FFT) patterns

[*] M. U. Khan,[+] L. Wang,[+] Z. Liu,[+] Z. Gao, S. Wang, H. Li, W. Zhang, M. Wang, Prof. Z. Wang, Prof. C. Ma, Prof. J. Zeng
Hefei National Laboratory for Physical Sciences at the Microscale
Hefei Science Center
National Synchrotron Radiation Laboratory & Synergetic Innovation Center of Quantum Information and Quantum Physics
Department of Chemical Physics
University of Science and Technology of China
Hefei, Anhui 230026 (P. R. China)
E-mail: zfwang15@ustc.edu.cn
zengj@ustc.edu.cn

[+] These authors contributed equally to this work.

Supporting information for this article can be found under: http://dx.doi.org/10.1002/anie.201602512.

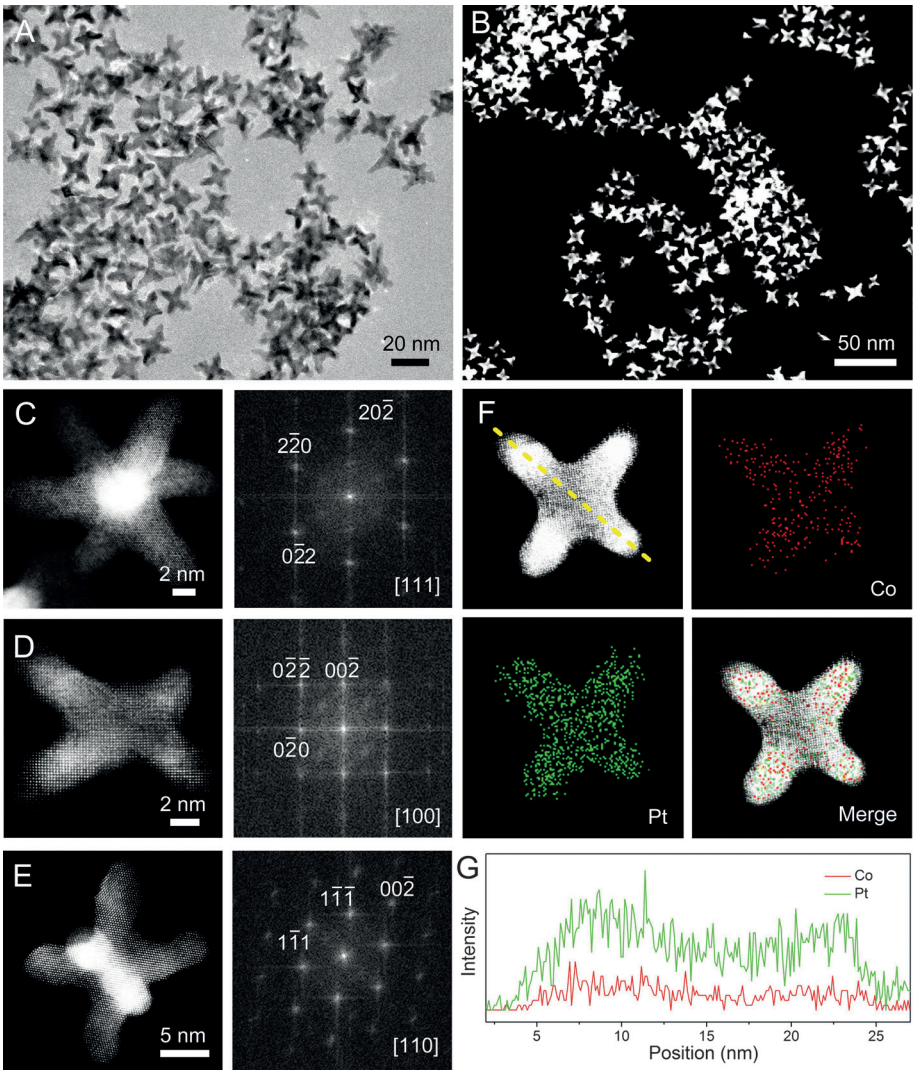

Figure 1. A, B) TEM and HAADF-STEM images of the Pt_3Co octapods. C–E) HAADF-STEM images and the corresponding FFT patterns of individual Pt_3Co octapods oriented along the [111], [100], and [110] axes, respectively. F) STEM image and STEM-EDX elemental mapping of an individual Pt_3Co octapod. Co red, Pt green. G) Compositional line profile of Pt and Co from a Pt_3Co octapod recorded along the yellow line shown in (F).

taken from an individual octapod oriented along three different zone axes ([100], [111], and [110]). As shown in Figure 1 C–E, the arms of the octapods were approximately 8 nm long and 3 nm thick. The composition and crystalline structure of the as-synthesized octapods were further analyzed by X-ray diffraction (XRD). The XRD pattern of the octapods can be indexed to a highly crystalline Pt_3Co phase with a face-centered cubic (fcc) structure (JCPDS No. 29-0499; see the Supporting Information, Figure S2). To analyze the structure and elemental composition of the Pt_3Co octapods, STEM energy-dispersive X-ray (EDX) elemental mapping images of an individual nanocrystal are presented in Figure 1 F, indicating the homogeneous distribution of both Pt and Co throughout the nanocrystal. The cross-sectional compositional line-scanning profile of the octapod in Figure 1 G further confirmed the complete overlap of both elements without significant segregation of the components. As revealed by inductively coupled plasma atomic emission spectroscopy (ICP-AES), the Pt/Co molar was 76:24, which is consistent with the XRD result. The procedure for the synthesis of the Pt_3Co nanocubes was similar to that for the Pt_3Co octapods except for changing the reaction temperature from 170 °C to 230 °C. As shown in Figure S3, Pt_3Co nanocubes with an average edge length of 8 nm and a narrow size distribution were thus obtained. For comparison, we also prepared Pt nanocubes and octapods according to reported methods.[11] These Pt nanocubes and octapods were uniform in size with average edge lengths of 13 and 8 nm, respectively (Figure S4).

The catalytic properties of the as-obtained Pt_3Co octapods and nanocubes in CO_2 hydrogenation were evaluated, and compared with those of Pt nanocrystals. All of the nanocrystals were loaded onto active carbon at a mass loading of 5 % (total metal amount), and exposed to UV/ozone at 80 °C for 30 min to clean the nanocrystal surface. After the UV/ozone treatment, the residual octanethiol used for synthesizing the Pt_3Co nanocrystals had been removed from the catalyst surface (Figure S5). A blank test was conducted with only active carbon added but no product was observed. When the reaction was catalyzed by Pt nanocubes (20 mg, 5 % mass loading) in a reaction flask pressurized with CO_2 (8 bar) and H_2 (24 bar) at 150 °C, about 2.9 mmol of methanol had been formed after 5 h (Figure 2 A). Under the same reaction conditions, the Pt octapods exhibited a slightly higher activity than the Pt nanocubes, with 3.1 mmol of methanol formed. For the Pt_3Co nanocubes and octapods, the catalytic activities were significantly higher, as approximately 7.9 and 17.3 mmol of methanol were generated, respectively (Figure 2 A). As a reference, we tested a commercial 5 % Pt/C catalyst, which yielded 3.4 mmol of methanol, which is comparable to the amount generated by the Pt nanocubes and octapods. To compare the catalytic activities more accurately, we calculated the turnover frequency numbers based on all metal atoms (denoted as TOF_{Metals}) of these catalysts. As shown in Figure 2 B, the TOF_{Metals} values of the Pt_3Co octapods, Pt_3Co nanocubes, Pt octapods, and Pt nanocubes were calculated to be 568, 261, 125, and 114 h^{-1},

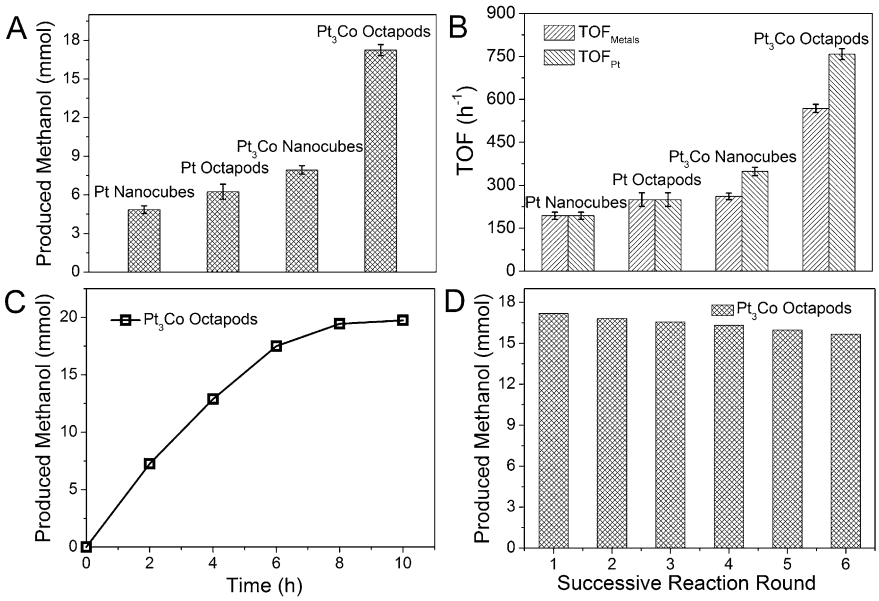

Figure 2. A) Product yields achieved with the Pt nanocubes, Pt octapods, Pt_3Co nanocubes, and Pt_3Co octapods (20 mg, 5% mass loading) in CO_2 hydrogenation at 150°C for 5 h. B) Comparison of the TOF_{Metal} and TOF_{Pt} numbers of different catalysts. C) Time course of the CO_2 hydrogenation catalyzed by Pt_3Co octapods (20 mg, 5% mass loading) at 150°C. D) Product yields achieved with Pt_3Co octapods (20 mg, 5% mass loading) over six rounds of successive reactions. Error bars represent the standard deviation from at least three independent measurements.

respectively. As the Pt atoms serve as the active sites, we further calculated the TOF numbers by solely taking the Pt atoms into account (TOF_{Pt}). The TOF_{Pt} values of the Pt_3Co octapods and nanocubes increased to 758 and 348 h^{-1}, respectively, whereas those of the Pt octapods and nanocubes naturally remained unchanged. Therefore, the Pt_3Co octapods display the highest activity among all tested catalysts, and the TOF_{Pt} of the Pt_3Co octapods was 2.2, 6.1, and 6.6 times higher than those of the Pt_3Co nanocubes, Pt octapods, and Pt nanocubes, respectively. Accordingly, the catalytic performance of the Pt_3Co octapods was worthy of further investigations by determining the product conversion with time. The methanol conversion amounted to almost 19.4 mmol after 10 h (Figure 2C). Furthermore, the stability of the Pt_3Co octapods was also studied by recycling the catalyst, as shown in Figure 2D. After six rounds, almost 91% of the original reactivity had been preserved. The high stability of the Pt_3Co octapods is of crucial importance for potential applications in industrial processes.

To explore the origin of the remarkable activity of the Pt_3Co octapods, we conducted density functional theory (DFT) calculations to investigate the electronic properties of the Pt and Pt_3Co nanocrystals. The Pt nanocubes, Pt octapods, Pt_3Co nanocubes, and Pt_3Co octapods were modeled as clusters with 172, 142, 172, and 142 atoms, respectively (Figure S6). As shown in Figure 3A and B, charge redistribution was observed in the Pt nanocubes and octapods. Specifically, considering an octapod as the combination of a cubic core with eight vertices protruding along the [111] directions from the corners of the nanocubes, we further investigated the charge distribution by dividing a Pt octapod into a cubic region and vertex region (Figure S7). As such, the negative charges in a Pt octapod are preferentially located in the vertex region where the accumulated charges per Pt atom were calculated to be −0.015 e, which corresponds to the sharp-tip effect. After the introduction of Co atoms, charge transfer between Pt and Co was observed owing to the difference in their electronegativities (Figure 3C, D). Obviously, all Pt atoms in the Pt_3Co nanocubes and octapods were negatively charged owing to the electron donation from Co to Pt. The average charges per Pt atom were −0.134 and −0.133 e for the Pt_3Co nanocubes and octapods, respectively, indicating a similar degree of charge transfer in the Pt_3Co nanocrystals regardless of their shapes (Table S1). For the Pt_3Co octapod, in particular, the Pt atoms in the vertex regions were more negatively charged with a charge of −0.142 e per Pt atom than those in the cubic region (−0.121 e). Our results demonstrate the favorable accumulation of negative charges in the vertices. It is worth noting that the sharp-tip effect is less obvious in the Pt octapods than in the Pt_3Co octapods because the tips in Pt octapods are not as sharp as those in the Pt_3Co octapods (see Figures 1 and S4). Therefore, the Pt atoms at the vertices in the Pt_3Co octapods are more negatively charged owing to the sharp-tip and alloy effects.

For further analysis of the electronic properties, we examined the Pt and Pt_3Co nanocrystals by X-ray photoelectron spectroscopy (XPS; Figure 4A and Figure S8). The binding energies of Pt $4f_{7/2}$ in the Pt nanocubes, Pt octapods, Pt_3Co nanocubes, and Pt_3Co octapods were found to be 71.4,

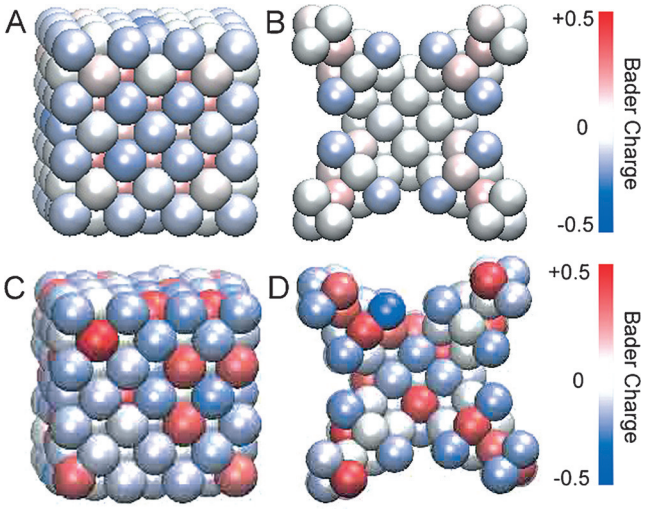

Figure 3. A–D) Bader charge analysis of the Pt nanocubes, Pt octapods, Pt_3Co nanocubes, and Pt_3Co octapods, respectively.

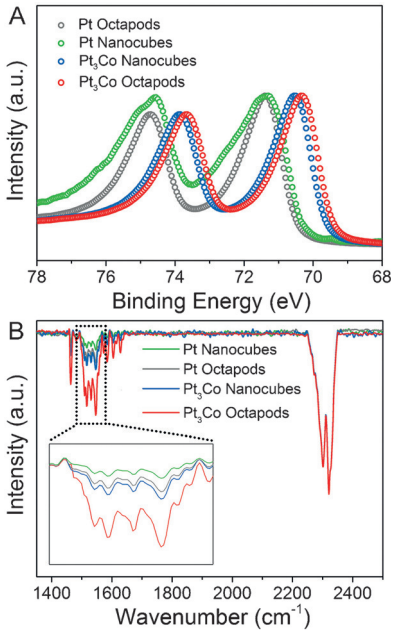

Figure 4. A) XPS and B) IRRAS spectra of the Pt nanocubes, Pt octapods, Pt_3Co nanocubes, and Pt_3Co octapods. The IRRAS spectra were obtained after the treatment of CO_2 gas at 150 °C.

71.3, 70.6, and 70.4 eV, respectively (Figure 4 A). The binding energy of the Pt nanocubes is very similar to that of the Pt octapods. Notably, the decrease in the Pt $4f_{7/2}$ energy in the Pt_3Co nanocrystals relative to that of the Pt nanocrystals implies that a charge transfer between Pt and Co has occurred in the Pt_3Co octapods and nanocubes, leading to negatively charged Pt atoms in these two alloy nanocrystals. Obviously, compared with the Pt_3Co nanocubes, more negative charges were accumulated on the surface Pt atoms in the Pt_3Co octapods owing to the greater Pt $4f_{7/2}$ binding energy. The large number of tips for the Pt_3Co octapods leads to a large proportion of surface area being in the vertex region where electrons are preferentially deposited. Collectively, the XPS results were in good agreement with the DFT calculations.

To investigate the role played by the negative charges in the activation of CO_2, the adsorption and activation of CO_2 molecules on these catalysts was analyzed by IRRAS. In the absence of catalyst, the spectrum of CO_2 exhibited two distinct peaks at 667 and 2350 cm^{-1}, which correspond to the bending and asymmetric stretching vibration modes of CO_2, respectively (Figure S9). In the presence of Pt-based catalysts, the bending mode (667 cm^{-1}) disappeared, along with the occurrence of a new band at approximately 1400–1700 cm^{-1}, indicating the presence of a carboxylate ($CO_2^{\delta-}$) species (Figure 4 B and Figure S10).[12] The generation of $CO_2^{\delta-}$ species is considered as the bottleneck in the activation of CO_2 as well as the chemical transformation of CO_2.[13] To compare the abilities of different catalysts to activate CO_2, we normalized the intensity of the band corresponding to the asymmetric stretching vibration of CO_2. The band intensity for $CO_2^{\delta-}$ increased on going from the Pt nanocubes to the Pt octapods, Pt_3Co nanocubes, and Pt_3Co octapods, which is consistent with the order of the negative charge densities of the Pt atoms in these catalysts (Figure 4 B). This order also corresponds to the sequence of the catalytic activities of the Pt_3Co and Pt nanocrystals. It is generally believed that a negatively charged surface is able to enhance the adsorption of CO_2 and therefore promote the activation of CO_2 molecules by forming $CO_2^{\delta-}$ intermediates.[4,13] Therefore, the higher negative charge density at the vertices of the Pt_3Co octapods promotes the activation of CO_2, which leads to an increase in the CO_2 hydrogenation activity.

In summary, we have combined sharp-tip and alloy effects to modulate the electronic properties of heterogeneous CO_2 hydrogenation catalysts and found that Pt_3Co octapods indeed display from superior catalytic activity. The highest TOF number of 758 h^{-1} was achieved using the Pt_3Co octapods, and is 2.2, 6.1, and 6.6 times higher than those of Pt_3Co nanocubes, Pt octapods, and Pt nanocubes, respectively. Both the branched morphology of the Pt_3Co octapods and the charge transfer between Pt and Co enabled the accumulation of negative charges in the vertices of the nanocrystals. IRRAS analysis confirmed that the high negative charge density of the Pt atoms in the vertices of the Pt_3Co octapods promoted the activation of CO_2 and accordingly enhanced the catalytic activity towards CO_2 hydrogenation to methanol. This work not only opens up new possibilities for designing efficient catalysts for CO_2 hydrogenation by electronic modulation, but also provides insights into strategies for modifying electronic properties.

Acknowledgements

This work was supported by the Collaborative Innovation Center of Suzhou Nano Science and Technology, the MOST of China (2014CB932700), the NSFC (21573206, 51371164, and 51132007), the Strategic Priority Research Program B of the CAS (XDB01020000), the Hefei Science Center, CAS (2015HSC-UP016), the Chinese Youth 1000 Talents Program, and the Fundamental Research Funds for the Central Universities. M.U.K. is also grateful for a generous CAS–TWAS president's fellowship. We also thank the Supercomputing Center at USTC for providing the computing resources.

Keywords: carbon dioxide · charge transfer · cobalt · hydrogenation · platinum

How to cite: *Angew. Chem. Int. Ed.* **2016**, *55*, 9548–9552
Angew. Chem. **2016**, *128*, 9700–9704

[1] a) F. Studt, I. Sharafutdinov, F. Abild-Pedersen, C. F. Elkjaer, J. S. Hummelshøj, S. Dahl, I. Chorkendorff, J. K. Nørskov, *Nat. Chem.* **2014**, *6*, 320–324; b) J. Hou, H. Cheng, O. Takeda, H. Zhu, *Angew. Chem. Int. Ed.* **2015**, *54*, 8480–8484; *Angew. Chem.* **2015**, *127*, 8600–8604; c) D. Gao, H. Zhou, J. Wang, S. Miao, F. Yang, G. Wang, J. Wang, X. Bao, *J. Am. Chem. Soc.* **2015**, *137*, 4288–4291; d) X. H. Liu, J. G. Ma, Z. Niu, G. M. Yang, P. Cheng, *Angew. Chem. Int. Ed.* **2015**, *54*, 988–991; *Angew. Chem.* **2015**, *127*, 1002–1005; e) Q. Xiang, B. Cheng, J. Yu, *Angew. Chem. Int. Ed.* **2015**, *54*, 11350–11366; *Angew. Chem.* **2015**, *127*, 11508–11524; f) J. C. Matsubu, V. N. Yang, P. Christopher, *J. Am. Chem.*

Soc. **2015**, *137*, 3076 – 3084; g) N. Kornienko, Y. Zhao, C. S. Kiley, C. Zhu, D. Kim, S. Lin, C. J. Chang, O. M. Yaghi, P. Yang, *J. Am. Chem. Soc.* **2015**, *137*, 14129 – 14135.

[2] a) S. Gao, Y. Lin, X. Jiao, Y. Sun, Q. Luo, W. Zhang, D. Li, J. Yang, Y. Xie, *Nature* **2016**, *529*, 68 – 71; b) M. Behrens, *Angew. Chem. Int. Ed.* **2014**, *53*, 12022 – 12024; *Angew. Chem.* **2014**, *126*, 12216 – 12218; c) Z. He, Q. Qian, J. Ma, Q. Meng, H. Zhou, J. Song, Z. Liu, B. Han, *Angew. Chem. Int. Ed.* **2016**, *55*, 737 – 741; *Angew. Chem.* **2016**, *128*, 747 – 751; d) A. Manzi, T. Simon, C. Sonnleitner, M. Döblinger, R. Wyrwich, O. Stern, J. K. Stolarczyk, J. Feldmann, *J. Am. Chem. Soc.* **2015**, *137*, 14007 – 14010; e) X. Meng, T. Wang, L. Liu, S. Ouyang, P. Li, H. Hu, T. Kako, H. Iwai, A. Tanaka, J. Ye, *Angew. Chem. Int. Ed.* **2014**, *53*, 11478 – 11482; *Angew. Chem.* **2014**, *126*, 11662 – 11666; f) Y. Zhao, G. Chen, T. Bian, C. Zhou, G. I. N. Waterhouse, L. Z. Wu, C. H. Tung, L. J. Smith, D. O'Hare, T. Zhang, *Adv. Mater.* **2015**, *27*, 7824 – 7831; g) C. Kim, H. S. Jeon, T. Eom, M. S. Jee, H. Kim, C. M. Friend, B. K. Min, Y. J. Hwang, *J. Am. Chem. Soc.* **2015**, *137*, 13844 – 13850.

[3] a) C. S. Li, G. Melaet, W. T. Ralston, K. An, C. Brooks, Y. F. Ye, Y. S. Liu, J. Zhu, J. Guo, S. Alayoglu, G. A. Somorjai, *Nat. Commun.* **2015**, *6*, 6538 – 6542; b) S. Moret, P. J. Dyson, G. Laurenczy, *Nat. Commun.* **2014**, *5*, 4017 – 4023; c) T. Kajiwara, M. Fujii, M. Tsujimoto, K. Kobayashi, M. Higuchi, K. Tanaka, S. Kitagawa, *Angew. Chem. Int. Ed.* **2016**, *55*, 2697 – 2700; *Angew. Chem.* **2016**, *128*, 2747 – 2750; d) I. Beinik, M. Hellström, T. N. Jensen, P. Broqvist, J. V. Lauritsen, *Nat. Commun.* **2015**, *6*, 8845 – 8853; e) G. A. Ozin, *Adv. Mater.* **2015**, *27*, 1957 – 1963; f) P. Z. Li, X. J. Wang, J. Liu, J. S. Lim, R. Zou, Y. Zhao, *J. Am. Chem. Soc.* **2016**, *138*, 2142 – 2145.

[4] a) Y. Li, S. H. Chan, Q. Sun, *Nanoscale* **2015**, *7*, 8663 – 8683; b) F. Solymosi, *J. Mol. Catal.* **1991**, *65*, 337 – 358; c) H. J. Freund, M. W. Roberts, *Surf. Sci. Rep.* **1996**, *25*, 225 – 273; d) R. N. Compton, P. W. Reinhardt, C. D. Cooper, *J. Chem. Phys.* **1975**, *63*, 3821 – 3827; e) J. Pacansky, U. Wahlgren, P. S. Bagus, *J. Chem. Phys.* **1975**, *62*, 2740 – 2744.

[5] F. Liao, Z. Zeng, C. Eley, Q. Lu, X. Hong, S. C. E. Tsang, *Angew. Chem. Int. Ed.* **2012**, *51*, 5832 – 5836; *Angew. Chem.* **2012**, *124*, 5934 – 5938.

[6] X. Yang, S. Kattel, S. D. Senanayake, J. A. Boscoboinik, X. Nie, J. Graciani, J. A. Rodriguez, P. Liu, D. J. Stacchiola, J. G. Chen, *J. Am. Chem. Soc.* **2015**, *137*, 10104 – 10107.

[7] J. Graciani, K. Mudiyanselage, F. Xu, A. E. Baber, J. Evans, S. D. Senanayake, D. J. Stacchiola, P. Liu, J. Hrbek, J. F. Sanz, J. A. Rodriguez, *Science* **2014**, *345*, 546 – 550.

[8] F. Calaza, C. Stiehler, Y. Fujimori, M. Sterrer, S. Beeg, M. Ruiz-Oses, N. Nilius, M. Heyde, T. Parviainen, K. Honkala, H. Häkkinen, H. J. Freund, *Angew. Chem. Int. Ed.* **2015**, *54*, 12484 – 12487; *Angew. Chem.* **2015**, *127*, 12661 – 12665.

[9] a) H. J. Zhang, T. Watanabe, M. Okumura, M. Haruta, N. Toshima, *Nat. Mater.* **2012**, *11*, 49 – 52; b) L. Wang, S. Zhao, C. Liu, C. Li, X. Li, H. Li, Y. Wang, C. Ma, Z. Li, J. Zeng, *Nano Lett.* **2015**, *15*, 2875 – 2880; c) J. Wu, L. Qi, H. You, A. Gross, J. Li, H. Yang, *J. Am. Chem. Soc.* **2012**, *134*, 11880 – 11883.

[10] a) S. Guo, D. Li, H. Zhu, S. Zhang, N. M. Markovic, V. R. Stamenkovic, S. Sun, *Angew. Chem. Int. Ed.* **2013**, *52*, 3465 – 3468; *Angew. Chem.* **2013**, *125*, 3549 – 3552; b) D. Kim, J. Resasco, Y. Yu, A. M. Asiri, P. D. Yang, *Nat. Commun.* **2014**, *5*, 4948 – 4955; c) B. Y. Xia, H. B. Wu, N. Li, Y. Yan, X. W. Lou, X. Wang, *Angew. Chem. Int. Ed.* **2015**, *54*, 3797 – 3801; *Angew. Chem.* **2015**, *127*, 3868 – 3872; d) M. Wang, L. Wang, H. Li, W. Du, M. U. Khan, S. Zhao, C. Ma, Z. Li, J. Zeng, *J. Am. Chem. Soc.* **2015**, *137*, 14027 – 14030.

[11] Y. Kang, J. B. Pyo, X. Ye, R. E. Diaz, T. R. Gordon, E. A. Stach, C. B. Murray, *ACS Nano* **2013**, *7*, 645 – 653.

[12] a) K. Mudiyanselage, S. D. Senanayake, L. Feria, S. Kundu, A. E. Baber, J. Graciani, A. B. Vidal, S. Agnoli, J. Evans, R. Chang, S. Axnanda, Z. Liu, J. F. Sanz, P. Liu, J. A. Rodriguez, D. J. Stacchiola, *Angew. Chem. Int. Ed.* **2013**, *52*, 5101 – 5105; *Angew. Chem.* **2013**, *125*, 5205 – 5209; b) O. Seiferth, K. Wolter, B. Dillmann, G. Klivenyi, H. J. Freund, D. Scarano, A. Zecchina, *Surf. Sci.* **1999**, *421*, 176 – 190.

[13] a) L. Dietz, S. Piccinin, M. Maestri, *J. Phys. Chem. C* **2015**, *119*, 4959 – 4966; b) T. Sommerfeld, H. D. Meyer, L. S. Cederbaum, *Phys. Chem. Chem. Phys.* **2004**, *6*, 42 – 45.

Received: March 11, 2016
Published online: May 2, 2016

